ELSEVIER

Journal of Nuclear Materials 283–287 (2000) 183–187

journal of nuclear materials

www.elsevier.nl/locate/jnucmat

# Study of He-bubble growth in α-particle implanted F82H-mod martensitic steel

R. Coppola [a,*], M. Magnani [b], R.P. May [c], A. Möslang [d], M. Valli [b]

[a] *ENEA-Casaccia SP050, CP 2400, 00100 Rome, Italy*
[b] *ENEA 'Clementel', via don Fiammelli 2, 40129 Bologna, Italy*
[c] *Institut Laue Langevin, BP 156, F-38042 Grenoble cedex 9, France*
[d] *Forschungszentrum, Institut für Materialforschung, P.O. Box 3640, D-76021 Karlsruhe, Germany*

**Abstract**

This paper presents the results of a small-angle neutron scattering (SANS) study of He-bubble growth in martensitic steel F82H-mod. The investigated samples had been homogeneously implanted with 400 appm He at 250°C, then submitted to 2 h annealings up to 975°C, together with a non-implanted sample of the same material (one for each temperature) serving as a reference to isolate the SANS signal arising from the He-bubbles. An as-implanted sample was also investigated together with its thermal reference. The He-bubble volume distributions, obtained from the SANS data and discussed with reference to uncertainties arising from background subtraction, show that the uniform distribution of the as-implanted sample, with bubbles approximately 15 Å in size, evolves during high temperature annealing into a bimodal one with a secondary population of bubbles as large as 100 Å approximately. 

## 1. Introduction

The results of a small-angle neutron scattering (SANS) study on the growth of He-bubbles in the martensitic steel F82H-mod are presented. This steel, which is one of the international reference materials for use in the 'first-wall' and blanket structures of fusion reactors [1], has a complex microstructural evolution. Irradiation defects, such as the He-bubbles, might be as small as 10 Å or less at blanket coolant inlet temperatures of 250–300°C. At irradiation temperatures of 400°C, typical size distributions of small cavities range from 20 to 100 Å in 9Cr–1MoVNb–2Ni and 12Cr–1MoVW–2Ni steels after HFIR irradiation, as shown by transmission electron microscopy (TEM) observation [2]. However at 250°C, cavity or bubble sizes appear sometimes to be below the TEM resolution limit of about 10–15 Å, as e.g., HFR irradiations of 9–12% CrMoVNb and 7–10% CrWVTa steels have shown [3]. SANS is therefore an appropriate technique in combination with TEM, as it is also shown by previous studies carried out on thermomechanically treated F82H-mod [4,5] and by preliminary results on He-bubble growth [6]. More specifically SANS data analyses have the potential to provide statistically significant He-bubble size and density distributions, which are essential to understand growth mechanisms and embrittlement effects.

## 2. Material characterization

The chemical composition of F82H-mod is: 8.0 Cr; 0.10 C; 0.16 Mn; 0.16 V; 2.0 W; 0.02 Ta wt%. After fabrication, the samples were submitted to the reference heat treatment: 40 min at 1040°C plus 2 h at 750°C. Samples approximately 1 $cm^2$ in surface and 0.4 mm thick had been homogeneously implanted at 250°C with 400 appm He, using 104 MeV α-particles at the high energy dual beam facility of the Forschungszentrum, Karlsruhe [7]. All but one (as-implanted sample) were submitted to 2 h thermal annealing (at 525°C, 825°C and 975°C) in high vacuum, together with non-implanted

* Corresponding author. Tel.: +39-06 3048 4724; fax: +39-06 3048 4747.
*E-mail address:* coppolar@casaccia.enea.it (R. Coppola).

0022-3115/00/$ - see front matter 
PII: S0022-3115(00)00221-X

samples of the same material (one for each temperature) serving as a reference to isolate the SANS signal arising from the He-bubbles. A sample of the same material submitted to thermal annealing at 250°C for a duration equivalent to the estimated implantation time (5 days) served as a reference for the as-implanted sample and was not further thermally treated. As mentioned in [6], it was preliminarily assumed that the microstructural effect produced at 250°C could be neglected in the high temperature tempered samples.

TEM pictures of He-bubbles in an F82H-mod sample submitted to the same kind of treatment as those investigated in the present work are reported in [6,8]. Since only a small fraction of bubbles might be visible in TEM micrographs, reliable density distributions can hardly be derived. Consequently, also an estimate of the bubble volume fraction from TEM data might be affected by large uncertainties, resulting in an apparent helium concentration which might deviate substantially from the nominally implanted one.

## 3. Experimental technique

Reference is made to previous work [4–6] for a presentation of the SANS technique applied to magnetic steels. The SANS measurements were carried out at the D11 instrument at the High Flux Reactor of the Institut Laue Langevin, Grenoble [9]. A sample-to-detector distance of 1.46 m and a wavelength $\lambda$ of 6 Å were used. This gave a $Q$-interval ranging from 0.04 to 0.25 Å$^{-1}$, which corresponds to particle sizes ranging from 10 to 80 Å approximately. $Q$ is the momentum transfer, $Q = (4\pi/\lambda)\sin\theta$, with $2\theta$ the full scattering angle. Calibration to absolute SANS cross-sections was obtained by measurement of 1 mm of water in a quartz cell. The data were treated by the ILL standard programs [10]. A horizontal magnetic field was applied perpendicular to the incoming neutron beam in order to fully align the magnetic moments in the sample. Thus, only nuclear scattering occurs in the horizontal plane, while nuclear and magnetic scatterings occur in the vertical one. Figs. 1(a) and (b) show the two-dimensional SANS cross-sections of the sample tempered at 975°C after implantation and of its thermal reference: the pattern of the implanted sample results from the superposition of the isotropic signal arising from the He-bubbles on the typical anisotropic pattern arising from the martensitic matrix, clearly visible in Fig. 1(a).

Since the He-bubbles are non-magnetic inhomogeneities imbedded in a magnetised matrix and the SANS difference between implanted and reference samples is the same for horizontal and vertical components (determined in sectors 10° wide), the distribution functions have been determined from the latter, which have better

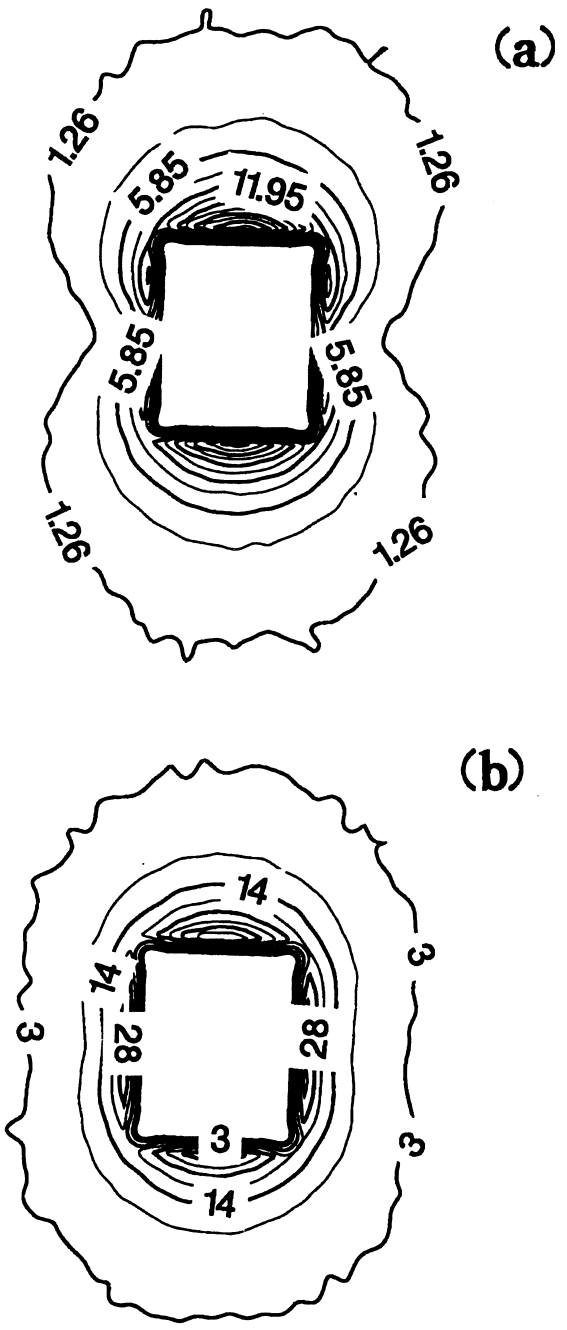


Fig. 1. Two-dimensional SANS cross-sections (cm$^{-1}$) of the F82H-mod sample tempered 2 h at 975°C (a) and of the sample implanted then tempered 2 h at 975°C (b). The applied field is parallel to the horizontal direction.

statistics. Each of the SANS nuclear and magnetic cross-sections can be written as

$$\frac{d\Sigma}{d\Omega}(Q) = (\Delta\rho)^2 \int_0^\infty N(R)V^2(R)|F(Q,R)|^2\,dR, \qquad (1)$$

where $N(R)\,dR$ is the number per unit volume of centres with a typical size between $R$ and $R + dR$, $V$ the volume, $|F(Q,R)|^2$ the form factor (assumed spherical in this case) and $(\Delta\rho)^2 = (\rho_{He} - \rho_{F82H})^2 = 4.833 \times 10^{21}$ cm$^{-4}$ is the 'contrast' or square difference in neutron scattering length density between He-bubbles, $\rho_{He} = 0.588 \times 10^{10}$ cm$^{-2}$ [11], and the F82H-mod matrix, $\rho_{F82H} = 7.54 \times 10^{10}$ cm$^{-2}$, the latter being determined from the chemical composition of F82H-mod [1,11].

As a first approximation, the contrast dependence on bubble radius [12] has been neglected, since it is evident from the small value of $\rho_{He}$ that very large changes of the He mass density would be necessary to lead to significantly different distributions; furthermore, as it is discussed in [12] and shown hereafter, much larger uncertainties are introduced by the experimental errors on SANS data and, consequently, on distributions. The volume distribution function is defined as

$$D(R) = N(R)R^3, \tag{2}$$

$N(R)$ was determined by transformation of Eq. (1) using the method described in [13] and more recently discussed in [14]. As already discussed in [6], a critical aspect of SANS measurements carried out on complex steels like F82H-mod is the background subtraction, that is the thermal references in this case. More specifically, the results presented in [4,5] have shown that any tempering following a single-step heat treatment (40 min at 1040°C) changes significantly the density of precipitates ($M_{23}C_6$ and, in the range 500–600°C, $M_2C$) with consequent changes in SANS cross-sections. In the present case, difficulties arising in background subtraction at high $Q$-values (in all $Q$-range at 525°C), are attributed to the fact that the thermal references had not exactly the same thermal history as the ones implanted at 250°C [6].

## 4. Results and discussion

Fig. 2 reports the differences in magnetic SANS cross-sections between implanted and reference samples at 250°C, 825°C and 975°C. It is clear that this correction becomes critical at high $Q$s and for the case of the as-implanted sample over the whole $Q$-range. The effects of different backgrounds on the volume distributions are shown in Figs. 3(a)–(c), referring to the sample tempered at 975°C. The best-fit distribution, minimising both $\chi^2$ and the error band, is the one of Fig. 3(b), obtained from the corresponding cross-section of Fig. 2 with a further background subtraction of 0.04 cm$^{-1}$ determined as an additional parameter. The distribution of Fig. 3(a) is obtained from the SANS data of the implanted sample without any background subtraction while Fig. 3(c) is the same as Fig. 3(b)

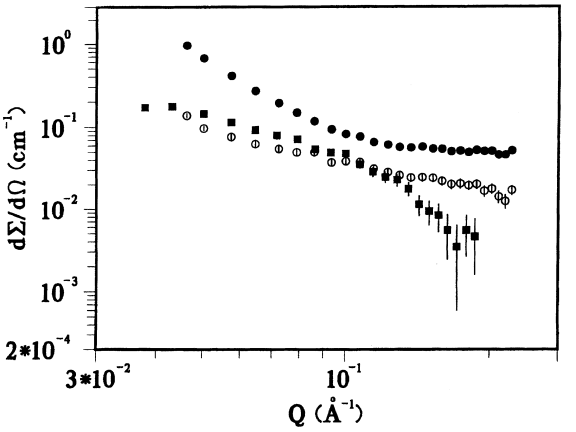


Fig. 2. Nuclear plus magnetic SANS cross-sections of the difference between implanted and reference samples for the following temperatures: 250°C (filled squares); 825°C (empty circles); 975°C (filled circles).

except an arbitrary increase in the background to 0.045 cm$^{-1}$. The structure of the $D(R)$s obtained in the three different cases is basically unchanged even if the background would be completely unknown (Fig. 3(a)), but different backgrounds can lead to important changes in intensity and the error band, particularly for low $R$s and outside the corresponding experimental $Q$-interval: as discussed elsewhere [6], it is clear that no quantitative information such as average radius can safely be determined for such small sizes.

Fig. 4 reports the three best-fit $D(R)$s obtained from the data of Fig. 2 [6], clearly showing that under high temperature tempering the initial distribution of He-bubbles present in the as-implanted sample evolves into a bimodal one. The corresponding volume fractions $\Delta V$, determined by integration of the $D(R)$s, are reported in Table 1 together with the average radii $R_b$. There is a fine agreement at 250° with the $R_b$ value determined from TEM, i.e., 16 Å [8]. Taking into account the best-fit error bands, typical errors on $\Delta V$ are 30–50%. However the $D(R)$s of Figs. 3(a) and (c) give volume fractions of 0.0968 and 0.0066, respectively, to be compared to the value of Table 1. Assuming that after high temperature annealing all implanted helium would be concentrated in

Table 1
He-bubble volume fraction, $\Delta V$ and average radius, $R_b$ (Å) from SANS analysis

| Annealing temperature (°C) | $\Delta V$ | $R_b$ |
|---|---|---|
| 250 | 0.0015 | 15 |
| 825 | 0.0079 | 5 |
| 975 | 0.0123 | 5[a] |

[a] With a secondary bubble population around 100 Å.

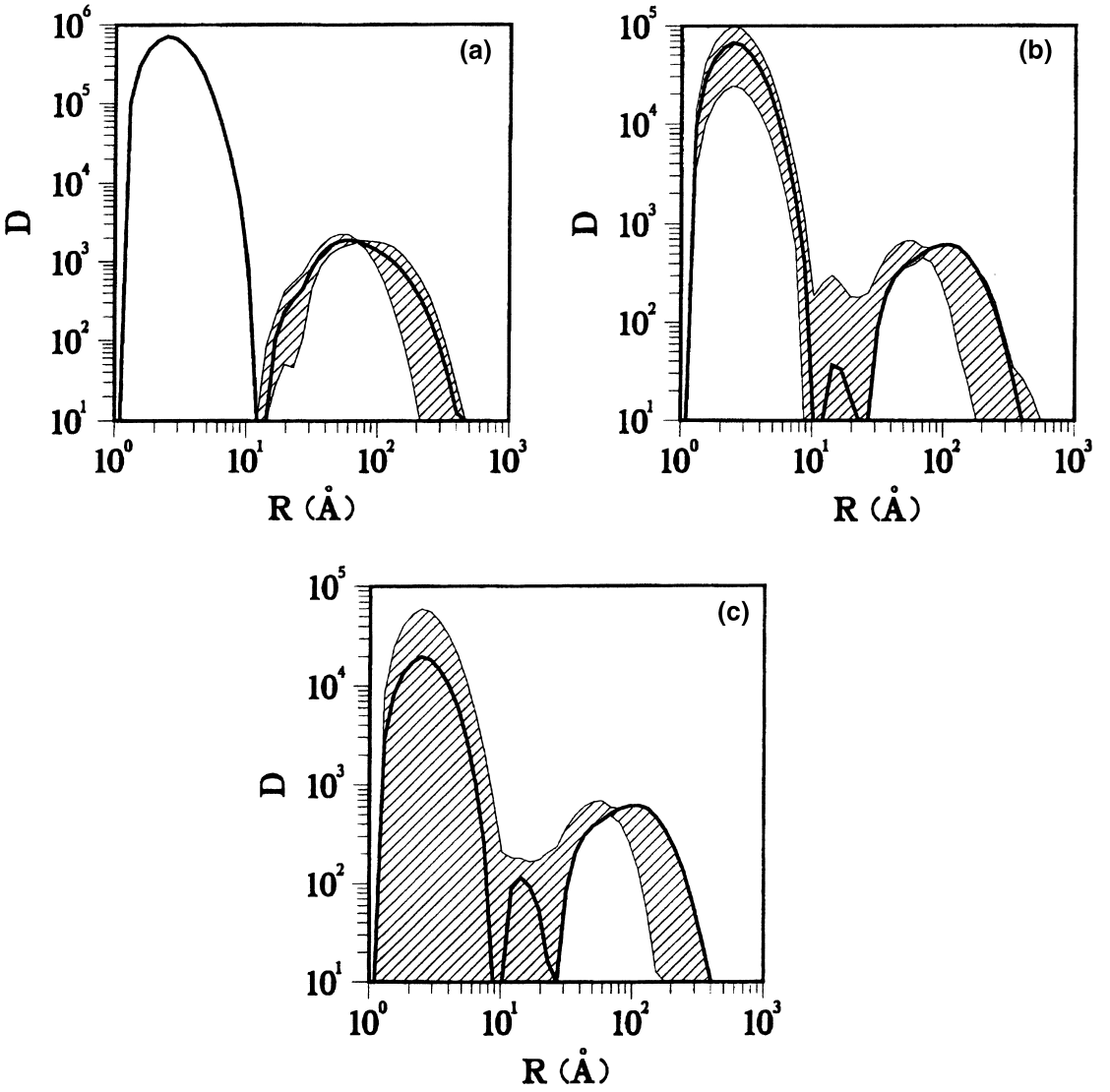


Fig. 3. $D(R)$ in $\text{Å}^{-1}$ (as defined in Eq. (2)) determined for the sample implanted at 250°C + tempered at 975°C: (a) without subtracting the thermal reference; (b) after subtraction of the reference, with an additional best-fit determined background noise of 0.04 $\text{cm}^{-1}$; (c) as in (b) but increasing the background noise to 0.045 $\text{cm}^{-1}$. The dashed areas represent the error band.

detectable equilibrium bubbles, $\Delta V$ should reflect the implanted helium concentration

$$C_{\text{He}} = \gamma \frac{\Delta V}{R_{\text{b}}} \frac{\Omega}{kT}, \tag{3}$$

where $\gamma$ is the bubble surface energy (related to He pressure $p_{\text{He}} = 2\gamma/R_{\text{b}}$ and assumed $\gamma = 1\ \text{J/m}^2$), $\Omega = 0.5 \times 2.87\ \text{Å}^3$ the atomic volume and $k = 1.38 \times 10^{-23}$ J/K. Inserting the values of Table 1 into Eq. (3) and neglecting the 'large' bubble population gives concentration values about one order of magnitude larger than the nominal one (400 appm He), which clearly implies that the effect of the background is underestimated in the data of Fig. 2 and, consequently, in the best-fit distribution of Fig. 3(b) and in its corresponding $\Delta V$. An accurate determination of bubble volume fraction requires therefore more reliable reference samples and a $Q$-range as large as possible. However these uncertainties on the absolute value of $\Delta V$ do not affect the reliability of the relative ones, showing an increase in bubble volume fraction with increasing temperature and providing a realistic picture of the He-bubble growth under post-implantation tempering.

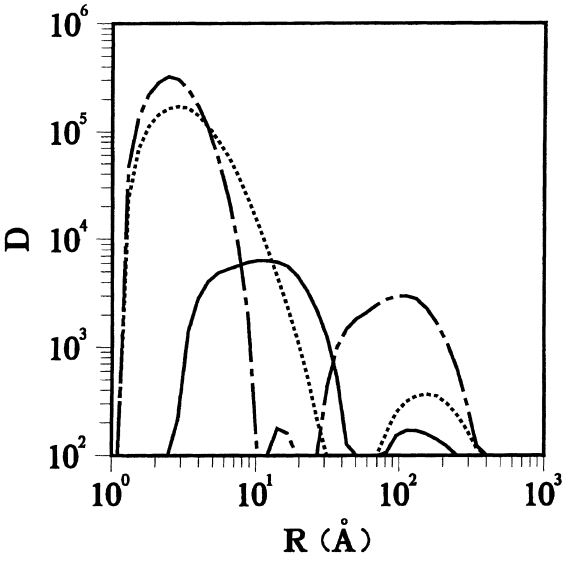


Fig. 4. He-bubble volume distribution functions $D(R)$ in $Å^{-1}$ at: 250°C (continuous line); 825°C (dotted line); 975°C (chained line).

## 5. Conclusion

The present results confirm the findings of preliminary work [6] carried out to investigate the growth of He-bubbles in implanted F82H-mod. A uniform bubble distribution produced during α-particle implantation at 250°C, with an average radius of 15 Å, develops during post-implantation tempering into a bimodal one. With increasing annealing temperature this bimodal distribution becomes more and more pronounced, but even at the highest temperature of 975°C the small bubble fraction appears still dominating with respect to bubble density. Owing to the complex microstructural evolution in the investigated steel, reference samples with exactly the same thermal history as the implanted ones are necessary for properly correcting background effects and, consequently, for a reliable determination of the absolute $\Delta V$ value. It is also foreseen to check by TEM bubble size and density and whether after tempering the bubbles are homogeneously distributed inside the grains or laths or whether they are mainly nucleated at larger precipitates or inner surfaces.

## References

[1] A. Hishinuma, A. Kohyama, R.L. Klueh, D.S. Gelles, W. Dietz, K. Ehrlich, J. Nucl. Mater. 258–263 (1998) 193.
[2] P.J. Maziasz, R.L. Klueh, in: N.H. Packan, R.E. Stoller, A.S. Kumar (Eds.), Effects of Radiation on Materials: 14th International Symposium, ASTM STP 1046, Philadelphia, vol. 1, 1989, p. 35.
[3] E.I. Materna-Morris, M. Rieth, K. Ehrlich, in: M.L. Hamilton, A.S. Kumar, S.T. Rosinski, M.L. Grossbeck (Eds.), Effects of Radiation on Materials: 19th International Symposium, ASTM STP 1366, West Conshohocken, vol. 1, 1999, p. 597.
[4] R. Coppola, M. Magnani, M. Stefanon, M. Valli, Report Subtask SM 6. 4, 1998, to be printed as ENEA Technical Report.
[5] R. Coppola, K. Ehrlich, M. Magnani, E. Materna-Morris, M. Valli, J. Nucl. Mater. 258–263 (1998) 1291.
[6] R. Coppola, M. Magnani, R.P. May, A. Möslang, J. Appl. Crystallogr., submitted.
[7] A. Möslang, S. Cierjacks, R. Lindau, in: B. Martin, K. Ziegler (Eds.), Proceedings of the 12th International Conference on Cyclotrons and their Applications Berlin 1989, World Scientific, London, 1991, p. 545.
[8] J. Bertsch, FZK Report 5984, 1997.
[9] P. Lindner, R.P. May, P.A. Timmins, Physica B 180&181 (1992) 967.
[10] R.E. Ghosh, S.U. Egelhaaf, A.R. Rennie, ILL Report ILL98GH14T, 1998.
[11] M.T. Hutchings, C.G. Windsor, in: K. Sköld, D.L. Price (Eds.), Neutron Scattering Part C, Academic, New York, 1987, p. 405.
[12] Qiang-Li, W. Kesternich, H. Schroeder, D. Schwahn, H. Ullmaier, Acta Metall. Mater. 38 (1990) 2383.
[13] M. Magnani, P. Puliti, M. Stefanon, Nucl. Instrum. and Meth. A 271 (1988) 611.
[14] R. Coppola, R. Kampmann, M. Magnani, P. Staron, Acta Mater. 46 (15) (1998) 5447.